



Development of a highly sensitive immuno-type fluorescence sensor utilising rare earth element-doped upconversion nanomaterials and graphene oxide for the detection of fenitrothion residues in food

Konghao Peng^{a,1} , Anqi Bai^{a,1}, Yue Wu^a, Shihan Wang^a, Heran Gao^a, Shurong Li^a, Lingyan Zhang^a, Min Jin^a, Wei Peng^{a,b,*} , Peijun Meng^{a,b,*} 

^a School of Public Health, Baotou Medical College, Inner Mongolia University of Science & Technology, Baotou 014040, China

^b Engineering Technology Center of Hygienic Inspection and Assessment of Inner Mongolia Autonomous Region, Baotou 014040, China

ARTICLE INFO

Keywords:

Fenitrothion
Fluorescence resonance energy transfer principle
Graphene oxide
Immune-based fluorescent sensor

ABSTRACT

Fenitrothion is an organophosphorus insecticide, and its residues in agricultural goods pose significant risks to human health. Therefore, prompt and precise identification of fenitrothion residues in agricultural commodities is of significant importance. This study employed rare earth element-doped upconversion nanomaterials (REs-UCNPs) and graphene oxide (GO) to develop an immune-based fluorescence sensor for fenitrothion detection. The nanomaterials NaYF₄:Yb,Er@NaYF₄ were synthesised via the solvothermal method, with polyacrylic acid modified on their surface through ligand exchange. NaYF₄:Yb,Er@NaYF₄ was conjugated with a monoclonal antibody using a glutaraldehyde cross-linking method, while GO was conjugated with the fenitrothion antigen. The precise interaction between the antigen and the antibody resulted in the binding of NaYF₄:Yb,Er@NaYF₄ to GO. When exposed to an excitation wavelength of 980 nm, GO could absorb the fluorescence emitted by NaYF₄:Yb,Er@NaYF₄ at 542 nm through the fluorescence resonance energy transfer mechanism. The fenitrothion pesticide could competitively bind to the monoclonal antibody with the antigen, thereby restoring the system's fluorescence. Under ideal conditions, the sensor's detection limit for fenitrothion was 0.081 ng/mL, with a linear range of 0.1–100 ng/mL. The spiking recoveries of fenitrothion in seven real samples varied from 91.79 % to 105.43 %, with relative standard deviations of 1.81–10.63 %. This study effectively developed a sensitive, accurate and specific immuno-type fluorescence sensor for the efficient and precise quantitative detection of fenitrothion in agricultural materials.

1. Introduction

Organophosphorus pesticides (OPs) are phosphorus-containing compounds utilised primarily for the prevention and control of plant diseases, pests and weeds. They are extensively employed in agriculture, forestry and animal husbandry across numerous countries, significantly contributing to enhanced agricultural yields and harvests. However, their widespread application may result in significant residues in the environment and agricultural products, causing contamination of soil, air and water [1,2]. Fenitrothion is an organophosphorus pesticide, and its extensive application has resulted in environmental residues that may endanger human health through food chain exposure [3,4]. Fenitrothion exerts its toxic effects by inhibiting acetylcholinesterase (AChE)

activity in neural tissues and other target organs, resulting in the accumulation of acetylcholine (ACh) and the subsequent overstimulation of muscarinic and nicotinic receptors, which manifests as excessive sweating, bronchospasm, hypotension and respiratory failure [5,6]. Even low levels of fenitrothion can pose significant risks to human health [7]. Considering the detrimental impacts of fenitrothion on human health, it is necessary to quantitatively evaluate and detect trace residues of fenitrothion in the environment and agricultural products.

Methods frequently employed for the detection of fenitrothion include chromatography [8], mass spectrometry [9], high-performance liquid chromatography-tandem mass spectrometry [10], electrochemistry [11], enzyme-linked immunosorbent assay [12] and enzyme inhibition [13]. Chromatography, mass spectrometry and high-performance

* Corresponding authors at: School of Public Health, Baotou Medical College, Inner Mongolia University of Science & Technology, Baotou 014040, China.

E-mail addresses: 2020400073@stu.btmc.edu.cn (W. Peng), 102006007@btmc.edu.cn (P. Meng).

¹ These authors contributed equally to this work.

liquid chromatography-tandem mass spectrometry are characterised by high precision; however, they involve complex sample pretreatment, has high costs and do not facilitate rapid analysis. Meanwhile, electrochemical methods offer low detection costs and enable swift analysis; however, their poor repeatability undermines the accuracy of the results. The enzyme inhibition method demonstrates commendable accuracy; however, its application in detecting OPs presents challenges. The approach can solely quantify the aggregate concentration of OPs and is incapable of identifying a specific pesticide. Hence, it is crucial to develop a sensitive, rapid, highly accurate and precise approach for detecting fenitrothion residues.

The fluorescence assay offers superior efficiency, fewer samples consumption and enhanced sensitivity relative to traditional techniques [14,15]. The performance of fluorescent sensors is affected by fluorescent probe materials: traditional small-molecule fluorescent probes are unstable and susceptible to interference by complex environments, which may affect the accuracy of sensor detection [16]; in the application of the quantum dots as a fluorescent probe, their high concentration causes biotoxicity and their luminescence efficiency is related to their synthesis process, which is highly demanding [17,18]. REEs-UCNPs are new fluorescent nanomaterials whose luminescence mechanism relies on the ability of ground-state ions to absorb low-energy photons and convert them into high-energy photons for emission. It pertains to anti-Stokes luminescence [19]. REEs-UCNPs exhibit chemical stability, prolonged luminescence lifetime, no autofluorescence interference, minimal photodamage to biological specimens and potential for surface modification [20]. Additionally, sensors utilising REEs-UCNPs as fluorescent probes demonstrate heightened sensitivity, precision and resistance to interference [21,22]. GO possesses a layered architecture, and numerous FRET-based fluorescence sensors are based on GO as a fluorescent receptor owing to its excellent dispersion, ability to undergo surface modification with various functional groups, substantial specific surface area and extensive UV absorption spectrum [23,24].

This study selected NaYF₄:Yb,Er@NaYF₄ as the fluorescence donor owing to its core-shell structure, which mitigates fluorescence bursts from surface defects in the nanomaterials, thereby increasing fluorescence intensity and enhancing the sensitivity of the fluorescence sensor [25]. GO was selected as the fluorescence acceptor to absorb the emitted fluorescence from the fluorescent probe. The specificity of conventional enzyme-inhibited OP sensors is inadequate [26], and the specific binding between the antigen and the antibody was utilised in this work to augment the sensors' specificity. The surface of NaYF₄:Yb,Er@NaYF₄ was modified with a fenitrothion monoclonal antibody and coupled with an antigen on the surface of GO. The fluorescence emitted from NaYF₄:Yb,Er@NaYF₄ was absorbed by GO through the specific interaction between the antigen and the antibody. Fenitrothion competitively reacted with the antigen, resulting in the dissociation of a portion of the fluorescent probe from the fluorescent receptor GO, thereby restoring the fluorescence of the sensor. The sensor's fluorescence was reinstated. To test this, a NaYF₄:Yb,Er@NaYF₄-GO immune-type nanofluorescence sensor was developed to quantitatively detect fenitrothion in real agricultural product samples.

2. Experimental section

2.1. Materials

The monoclonal antibody, antigen conjugate, and fenitrothion standard were acquired from Shandong Lvdu Bio-technique Industry (Shandong, China). Twenty-four organophosphorus pesticide standards were acquired from Tianjin Alta Scientific Co., Ltd. (Tianjin, China). Graphene oxide powder (>99 %), YCl₃·6H₂O (99.99 %), YbCl₃·6H₂O (99.9 %), ErCl₃·6H₂O (99.5 %), Oleic acid (OA), 1-Octadecene (>90 %), Sodium hydroxide (97 %), Ammonia (25 %-28 %), Methanol (99.5 %), Polyacrylic acid (PAA), 1-Ethyl-(3-dimethylaminopropyl) carbodiimide hydrochloride (98 %) (EDC), N-hydroxythiosuccinimide sodium salt

(98 %) (NHS), Tween 20, Alginate (99 %), and Bovine serum albumin (>98 %) (BSA) were acquired from Shanghai Aladdin Biochemical Technology Co., Ltd. (Shanghai, China). The experiment utilized ultra-pure water obtained from Hangzhou Wahaha Group Co., Ltd (Zhejiang, China).

2.2. Instruments

The microstructure and morphology of upconversion nanoparticles (UCNPs) and GOs were observed using a JEM-2100F field emission transmission electron microscope (TEM, JEOL Ltd, Japan). The microscopic surface structure and morphology of the materials were observed using a ZEISS Gemini 300 scanning electron microscope (SEM, Carl Zeiss AG, Germany). The crystal structures of UCNPs and GO were analyzed by Smartlab 9 X-ray diffraction (XRD, Rigaku Corporation, Japan). The materials were analyzed for chemical bonds and functional groups using the Nicolet iS5 Fourier-transform infrared spectrometer (FTIR, Thermo Scientific, USA). The upconversion excitation light was provided using the MDL-H-980 980 nm near-infrared laser (Fine Mechanics and Physics, Chinese Academy of Sciences, China). The fluorescence intensity of the system was measured by F-4600 Hitachi molecular fluorescence spectrometer (Hitachi, Japan). The absorption spectra of materials are tested using the UV-2600i Ultraviolet-Visible Spectrophotometer (UV-Vis, Shimadzu Corporation, Japan). The Zeta potential values of materials were tested using a BeNano 90 Zeta Nanoparticle Size and Zeta Potential Analyzer (Zeta, Dandong Bettersize instruments Ltd, Liaoning, China).

2.3. Synthesis of NaYF₄:Yb,Er

NaYF₄:Yb,Er was synthesised through the solvothermal method [27] by placing 0.2366 g of YCl₃·6H₂O, 0.0775 g of YbCl₃·6H₂O and 0.0076 g of ErCl₃·6H₂O in a three-necked flask, adding 6 mL of OA and 18 mL of 1-Octadecene and subsequently raising the temperature to 160 °C under magnetic stirring for 30 min. The temperature was raised to 160 °C with magnetic stirring, maintained for 30 min and then cooled to ambient temperature to obtain a homogeneous and transparent faint yellow solution. NaOH (0.1000 g) and NH₄F (0.1482 g) were diluted in 10 mL of methanol, incrementally added to a three-necked flask and agitated for 30 min. The mixture was subsequently heated to 100 °C for 30 min to evaporate the methanol, after which it was placed in a condenser tube where the temperature was raised to 300 °C under flowing argon for 1.5 h. After the reaction, the product was washed three times with a designated amount of cyclohexane and ethanol. The synthesised NaYF₄:Yb,Er was freeze-dried to obtain a powdered form. The powder samples were examined by TEM, SEM, XRD, FTIR and fluorescence spectroscopy with 980 nm excitation light.

2.4. Synthesis of NaYF₄:Yb,Er@NaYF₄

NaYF₄:Yb,Er@NaYF₄ was synthesized using solvothermal method [25]. YCl₃·6H₂O (0.2 mmol), OA (4.8 mL) and 1-Octadecene (12 mL) were mixed in a three-necked flask at a constant temperature of 160 °C for 60 min under an argon atmosphere, resulting in a transparent solution. After cooling to room temperature, 1 mmol of NaYF₄:Yb,Er dissolved in 4 mL of cyclohexane was added, followed by the addition of 0.0300 g of NaOH and 0.0444 g of NH₄F dissolved in 3 mL of methanol. The solution was subsequently heated to 100 °C and maintained for 20 min, followed by heating to 300 °C under argon gas for 1.5 h. On completion of the reaction, the synthesised NaYF₄:Yb,Er was washed three times with cyclohexane and ethanol and then freeze-dried to obtain a powder. The powder samples were characterised by TEM, SEM, XRD, FTIR and fluorescence spectroscopy under 980 nm excitation light irradiation.

2.5. Preparation of $\text{NaYF}_4\text{:Yb,Er@NaYF}_4\text{@PAA}$

PAA was coated on the $\text{NaYF}_4\text{:Yb,Er@NaYF}_4$ surface using the ligand exchange method [28]. $\text{NaYF}_4\text{:Yb,Er@NaYF}_4$ (30 mg) was dissolved in 4 mL of trichloromethane. In a three-necked flask, 200 mg of PAA was dissolved in 8 mL of purified water and 4 mL of UCNPs chloroform solution was gradually added into the three-necked flask and magnetically stirred for 24 h. Subsequently, the resultant mixed solution was centrifuged for 30 min at 14,000 rpm. Following centrifugation, the supernatant was removed, and the precipitate was washed three times with water and anhydrous ethanol and subsequently lyophilised to yield $\text{NaYF}_4\text{:Yb,Er@NaYF}_4\text{@PAA}$. The powder samples were collected and analysed by TEM, SEM, XRD, FTIR and fluorescence spectroscopy.

2.6. Carboxylation of GO

GO-COOH was prepared by the method of chloroacetic acid addition [29]. GO (25 mg) was dissolved in 25 mL of distilled water, sonicated for 30 min to achieve dispersion, then added with 1.5 g of sodium hydroxide and stirred until dissolved. Chloroacetic acid (1 g) was added, and the resultant solution was sonicated for 1 h. The mixture was agitated at ambient temperature overnight. The reaction mixture was centrifuged, washed thrice with water and anhydrous ethanol and then lyophilised overnight to obtain GO-COOH powder.

2.7. $\text{NaYF}_4\text{:Yb,Er@NaYF}_4\text{@PAA}$ conjugated with fenitrothion monoclonal antibody

UCNPs-mAb were prepared by amidation reaction [30]. To a 1 mL aqueous solution of $\text{NaYF}_4\text{:Yb,Er@NaYF}_4\text{@PAA}$ (0.5 mg/mL), 0.5 mg NHS and 0.75 mg EDC were added to activate the carboxyl groups, and the solution was vortexed at 800 rpm for 20 min, followed by centrifugation at 9000 rpm for 10 min to precipitate the active pellet, with 95 % of the supernatant discarded. The precipitate was sonicated with 1 mL of PBS at pH 7.4 for 5 min. The aforementioned activation solution of UCNPs (500 μL) was aliquoted, to which 10 μL (2 mg/mL) of fenitrothion monoclonal antibody was added. The mixture was agitated at 250 rpm for 2 h, followed by addition of 50 μL of 1 % BSA to seal it for 30 min. Subsequently, it was centrifuged at 11,000 rpm for 10 min, after which the supernatant was discarded, and the precipitate was reconstituted in a PBS solution (pH = 7.4) containing 1 % BSA (w/v), 1 % alginate (w/v) and 0.1 % Tween-20 (v/v). The prepared UCNPs-mAb (0.5 mg/mL) was preserved at 4 °C.

2.8. Antigen-coupled carboxylated GO

GO-COOH-Ag were prepared by amidation reaction [31]. GO-COOH (1 mg) was dissolved in 1 mL of MES (pH = 5.2) following the addition of 10 mg of NHS and 10 mg of EDC. The carboxyl groups were activated by vortex mixing for 30 min at 800 rpm. The reaction was centrifuged. Then, the supernatant was removed, and the centrifuge was rinsed twice with 1 mL of PBS. The activation product was harvested and solubilised in 10 mL of PBS at a concentration of 0.1 mg/mL. 1 mL of the aforementioned solution was placed in a three-necked flask, to which 20 μL (2.5 mg/mL) of fenitrothion antigen was added, and the mixture was agitated at 4 °C overnight. Following agitation, the GO antigen conjugate was washed and centrifuged twice with PBS at 11,000 rpm for 10 min, and the resultant GO antigen conjugate was dissolved in 1 mL of PBS to yield GO-COOH-Ag at a concentration of 0.1 mg/mL.

2.9. Optimisation of the reaction conditions for immunoassay-based fluorescent sensors

The ideal parameters for detecting fenitrothion using the UCNPs-mAb + GO-Ag immuno-type nanofluorescent sensor were established by analysing the variations in fluorescence bursting efficiency and

fluorescence recovery efficiency across different concentrations of fenitrothion monoclonal antibodies, fenitrothion antigens, types of buffer solutions, pH levels, durations of reaction fluorescence bursting and competitive fluorescence recovery times. The fluorescence burst efficiency is defined as $(F_0-F_1)/F_0$, while the fluorescence recovery efficiency is calculated as $(F_2-F_1)/F_2$, where F_0 is the fluorescence value of UCNPs-mAb, F_1 is the fluorescence value of UCNPs-mAb + GO-Ag and F_2 is the fluorescence value of UCNPs-mAb + GO-Ag + OP.

2.10. Construction of an immune-based fluorescence sensor

Under optimal conditions (a system pH of 7.4, a reaction fluorescence burst time of 40 min, a competition fluorescence recovery time of 25 min, in PBS buffer solution, an antibody concentration of 2.0 mg/mL and an antigen concentration of 2.5 mg/mL), a mixture of 500 μL of $\text{NaYF}_4\text{:Yb,Er@NaYF}_4\text{@PAA}$ -mAb (0.5 mg/mL) and 500 μL of GO-COOH-Ag (0.1 mg/mL) were allowed to react for 40 min, followed by addition of 200 μL of varying concentrations of fenitrothion (0.1, 1, 10, 20, 40, 50, 80, 100, 150, 200 ng/mL) into the sensor. The upconverted fluorescence was measured at varying concentrations of fenitrothion. Fluorescence difference (F_2-F_1 , where F_1 is the fluorescence value of UCNPs-mAb + GO-Ag and F_2 is the fluorescence value of UCNPs-mAb + GO-Ag + fenitrothion) was utilised as the vertical axis, while the concentration of fenitrothion served as the horizontal axis. Fluorescence difference was subsequently graphed against the concentration of fenitrothion.

2.11. Specificity and anti-interference experiments

This study selected 25 different types of pesticides, such as organophosphorus, organochlorine, nicotine, pyrethroid, benzimidazole and bipyridine. In accordance with the procedure outlined in Section 2.8, 25 distinct pesticide types, each at a concentration of 100 ng/mL, were introduced, and the resultant fluorescence variations for each pesticide were analysed to assess the specificity of the immunofluorescence sensor.

To examine the sensor's immunity, metal ions, anions, amino acids and vitamins were selected as interfering components. The detection method outlined in Section 2.8 was employed, where in 200 μL of fenitrothion at a concentration of 100 ng/mL was introduced to the sample, followed by the addition of 200 μL of interfering substances at a concentration of 10 $\mu\text{g/mL}$. The influence of 17 interfering compounds on the detection of fenitrothion pesticide by the sensor was examined, and the immunofluorescence sensor was studied.

2.12. Pretreatment and spiking recovery tests of real samples

Green tea, rice, millet, lettuce, cucumber, apple and pear were chosen as test samples. The samples were ground or crushed, and 1 g of each was extracted with 3 mL of acetone, filtered and subsequently diluted. Fenitrothion pesticide was not detected in any of the samples. The extract was then diluted and combined with a fenitrothion standard, prepared as a solution with concentrations of 1, 40 and 80 ng/mL for testing. The precision of the immunofluorescence sensor on real samples was evaluated by the proposed sensor.

3. Results and discussion

3.1. Mechanism of the immuno-type fluorescent sensor

Fig. 1 illustrates a schematic representation of the immuno-type fluorescence sensor's mechanism. The fenitrothion antigen was immobilized to the GO surface through glutaraldehyde cross-linking. A monoclonal antibody targeting fenitrothion was conjugated to the surface of $\text{NaYF}_4\text{:Yb,Er@NaYF}_4\text{@PAA}$ by glutaraldehyde cross-linking. The specific binding between the antigen and the antibody reduces the

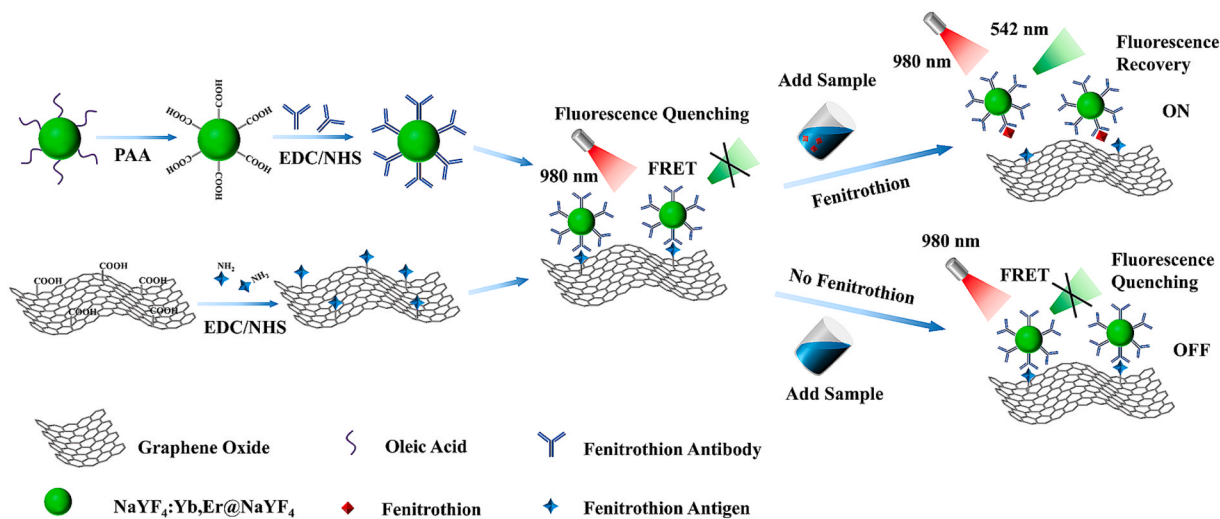


Fig. 1. Schematic representation of the immunofluorescent sensor's principle.

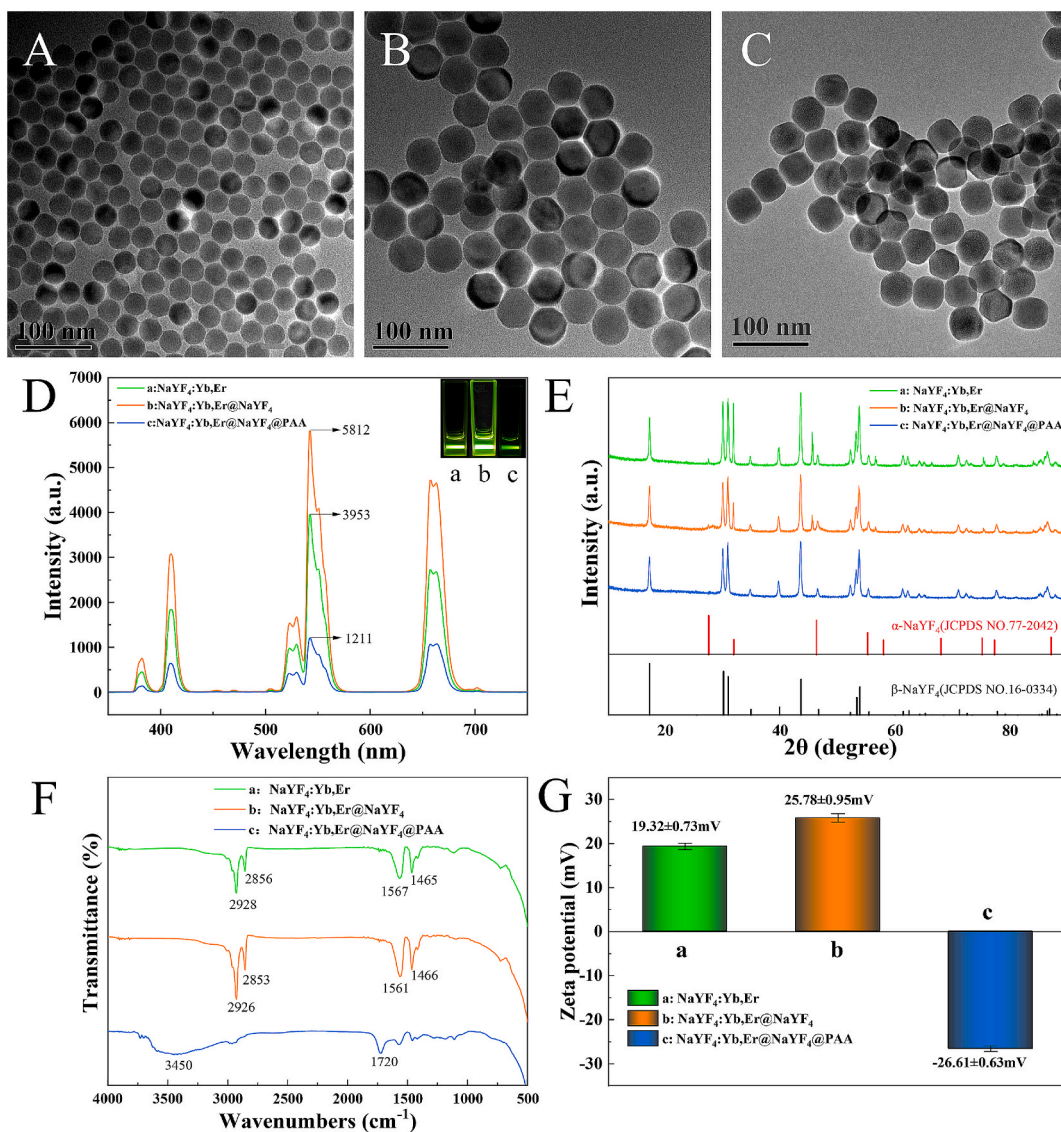


Fig. 2. TEM images of $\text{NaYF}_4:\text{Yb,Er}$ (A), $\text{NaYF}_4:\text{Yb,Er}@NaYF_4$ (B) and $\text{NaYF}_4:\text{Yb,Er}@NaYF_4@PAA$ (C). Fluorescence spectra (D), XRD (E), FTIR spectra (F) and Zeta potentials (G) of $\text{NaYF}_4:\text{Yb,Er}$ (a), $\text{NaYF}_4:\text{Yb,Er}@NaYF_4$ (b) and $\text{NaYF}_4:\text{Yb,Er}@NaYF_4@PAA$ (c).

distance between the fluorescence acceptor GO and the fluorescence donor NaYF₄:Yb,Er@NaYF₄@PAA, thereby fulfilling the criteria for fluorescence resonance energy transfer (FRET) and resulting in a significant decrease in system fluorescence [32,33]. Fenitrothion, being a small molecule with a strong antigen binding capacity, competes with the fluorescence acceptor for the fluorescence donor. As fenitrothion binds to the fluorescence donor, it detaches from the fluorescence acceptor, resulting in fluorescence recovery within the system and the fluorescence “ON” [34]. The concentration of fenitrothion in the sample correlates positively with the extent of fluorescence recovery; thus, a higher concentration yields a greater fluorescence recovery value. Conversely, in the absence of fenitrothion in the sample, there is no competition for the fluorescence donor, resulting in a fluorescence value that remains relatively constant and the fluorescence “OFF”. Utilising this idea, we developed an immunofluorescence sensor for the quantitative detection of fenitrothion.

3.2. Characterisation of NaYF₄:Yb,Er@NaYF₄@PAA nanomaterials

Characterization of NaYF₄:Yb,Er (A), NaYF₄:Yb,Er@NaYF₄ (B) and NaYF₄:Yb,Er@NaYF₄@PAA (C) using TEM and SEM. The results are shown in Fig. 2A-C and S1A-C. All three materials exhibit hexagonal crystalline structures, demonstrating uniform size and adequate dispersion. Fig. S2 illustrates that the average particle size of NaYF₄:Yb,Er was 30.34 nm, that of NaYF₄:Yb,Er@NaYF₄ was 48.90 nm and that of NaYF₄:Yb,Er@NaYF₄@PAA measured 48.93 nm. The particle size of the NaYF₄:Yb,Er@NaYF₄ core-shell nanomaterials increased by approximately 18 nm compared to NaYF₄:Yb,Er, and the particle size of the nanomaterials remained constant after the application of polyacrylic acid via the ligand exchange method.

Fluorescence spectroscopy, XRD, FTIR and zeta potential tests were used to characterize the fluorescence properties, crystal conformation, surface functional group conditions and zeta potential values of the three materials. The emission fluorescence spectra of three materials under 980 nm excitation light are depicted in Fig. 2D. All three materials exhibit yellowish-green fluorescence, with peak emission wavelengths at 410, 530, 542 and 658 nm. The maximum value at 542 nm was the highest; hence, the 542 nm fluorescence value was utilised as the sensor's detecting signal. The core-shell structure of NaYF₄:Yb,Er@NaYF₄ (b) enhances the sensitivity of the fluorescence sensor compared to NaYF₄:Yb,Er (a) by mitigating fluorescence bursts generated by surface defects in the nanomaterials, hence increasing the fluorescence value. This improvement is consistent with previous study [25]. The fluorescence value of the nanomaterial NaYF₄:Yb,Er@NaYF₄@PAA (c) diminishes following the application of polyacrylic acid coating. Fig. 2E presents the XRD patterns of three materials. The positions of the peaks for all three nanomaterials correspond to the standard card (JCPDS No. 16-0334), confirming that they all exhibit a hexagonal crystalline structure. Fig. 2F presents the FTIR spectra, illustrating the IR characteristic peaks of NaYF₄:Yb,Er (a) and NaYF₄:Yb,Er@NaYF₄ (b), which correspond to the characteristic peaks of OA. Notably, the characteristic peaks of OA are absent in the IR spectra of NaYF₄:Yb,Er@NaYF₄@PAA (c) following the application of PAA coating. The distinctive peaks of carboxylic acid at 3450 and 1720 cm⁻¹ further confirm the effective alteration of PAA, which is consistent with previous FTIR characterization study of PAA-functionalized nanomaterials [35]. In Fig. 2G, the zeta potential of NaYF₄:Yb,Er (a) is 19.32 ± 0.73 mV, that of NaYF₄:Yb,Er@NaYF₄ (b) is 25.78 ± 0.95 mV and that of NaYF₄:Yb,Er@NaYF₄@PAA (c) is -26.61 ± 0.63 mV. The zeta potential value of the material becomes negative and increases in absolute magnitude following the alteration of polyacrylic acid, demonstrating that NaYF₄:Yb,Er@NaYF₄@PAA is effectively distributed in pure aqueous media without agglomeration or sedimentation. Fig. S3 illustrates the fluorescence performance of NaYF₄:Yb,Er@NaYF₄@PAA remains stable in pure water medium, with the fluorescence value consistently unaltered throughout time. The above results indicate NaYF₄:Yb,Er@NaYF₄@PAA

has been successfully prepared.

3.3. Characterisation of GO before and after carboxylation

Fig. S4 shows that the structures of both GO and GO-COOH are lamellar. Fig. S5A presents the XRD patterns of GO before and after carboxylation. The layer spacing of GO was determined using Bragg's equation [36], revealing diffraction peaks at 2θ = 10.09° with a layer spacing of d = 0.88 nm for GO and at 2θ = 9.72° with a layer spacing of d = 0.91 nm for GO-COOH. This alteration is attributed to the increased layer spacing between GO lamellas following the incorporation of carboxyl groups. Fig. S5B displays the Raman spectra of GO and GO-COOH. Both GO (a) and GO-COOH (b) exhibit two prominent Raman absorption peaks: the D-band, indicative of the degree of ordering in the conjugated structure, situated at 1350 cm⁻¹, and the G-band, associated with graphite plane vibrations, located near 1600 cm⁻¹. The intensity ratios of the D-band to the G-band for GO (a) and GO-COOH (b) (ID/IG, indicative of graphene defects) are 0.90 and 0.96, respectively. The elevation of this value demonstrates that the incorporation of chloroacetic acid enhances the disorder inside GO, our conclusions are supported by existing research [37]. Fig. S5C shows the infrared spectra of GO and GO-COOH, indicating that GO exhibits a distinctive absorption peak for -OH at around 3300 cm⁻¹ post-carboxylation, along with typical peaks for C=O and sp² hybridised C=C functional groups at 1732 and 1591 cm⁻¹, respectively. The aforementioned data substantiate the effective synthesis of GO-COOH, these characteristic infrared absorption bands are consistent with previous report on carboxylation of GO [38].

Fig. S5D shows the UV absorption spectrum of GO within the 200–800 nm wavelength range and the emission fluorescence spectrum of NaYF₄:Yb,Er@NaYF₄@PAA under 980 nm excitation light. By fulfilling one of the criteria for FRET, GO can function as a fluorescence receptor, resulting in the quenching of the nanomaterial's fluorescence [22].

3.4. Feasibility analysis of fluorescent sensors

Fig. S6A shows the UV absorption spectra of GO-Ag (a), Ag (b) and GO (c). The UV absorption peaks of GO, following the modification with the fenitrothion antigen, exhibited typical peaks of the antigen, thereby confirming the successful modification of the antigen on the surface of GO. Fig. S6B shows the UV absorption spectra of UCNPs (a), mAb (b) and UCNPs-mAb (c). Following the modification of UCNPs with the fenitrothion monoclonal antibody, the UV absorption peaks exhibited characteristic features of the antibody, confirming the successful modification of mAb onto the surface of UCNPs, this conclusion is consistent with previous study [39]. Fig. S7 shows the fluorescence spectra of UCNPs-mAb (a), UCNPs-mAb + GO-Ag (b) and UCNPs-mAb + GO-Ag + OP (c). The fluorescence of the sensor system diminished on introduction of GO-Ag and reaction with UCNPs-mAb, subsequently recovering on addition of a specific quantity of fenitrothion standard. The fluorescence variation principle of the system aligns with the theoretical framework of FRET and competitive reactions, resulting in fluorescence recovery, thus demonstrating the viability of the immunological fluorescence sensor.

3.5. Optimisation of the reaction conditions for fluorescence sensors

To investigate the optimal concentration ratio of GO coupled antigen, the concentration of fenitrothion actually coupled to GO was determined by using the Coomassie blue staining solution method [31]. As shown in Fig. S8A and Fig. S8B, the discussion of experimental results can be found in the supplementary material. The optimal coupling concentration of antigen was 2.5 mg/mL.

Fig. 3A illustrates the fluorescence burst value of the fluorescence sensor system across various pH environments, maintaining constant reaction conditions. The fluorescence burst value attains its peak at a pH

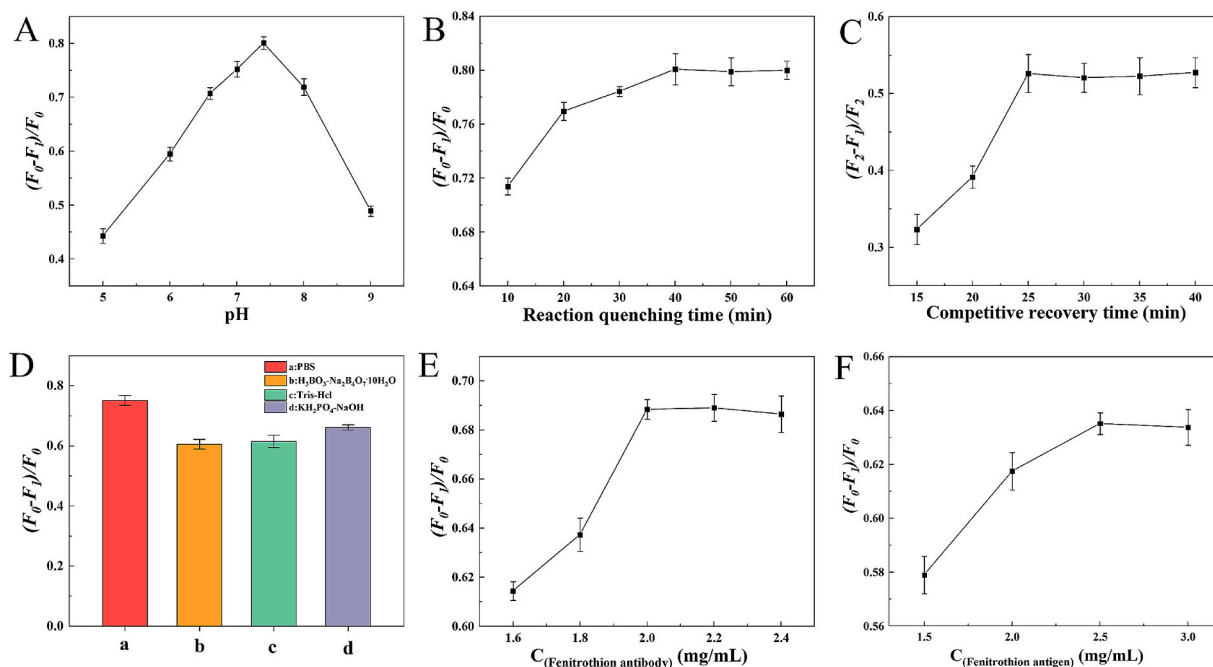


Fig. 3. Optimisation of parameters for various reaction conditions: pH (A), reaction burst duration (B), competition recovery duration (C), buffer solution classification (D), antibody concentration (E) and antigen concentration (F).

of 7.4, indicating that this pH level is optimal for the reaction. Fig. 3B illustrates the fluorescence burst values of the fluorescence sensor system at varying reaction periods while maintaining constant the other reaction circumstances. The fluorescence burst efficiency of the sensor escalates over time, achieving maximum fluorescence burst value at 40 min, at which point it stabilises; thus, the best reaction burst duration is 40 min. Fig. 3C illustrates that, while maintaining constant reaction conditions, the fluorescence competition recovery efficiency of the sensor escalates over time. At a reaction duration of 25 min, the fluorescence intensity of the sensor system attains its peak and approaches stabilisation, indicating that the optimal competition fluorescence recovery time is 25 min. Fig. 3D illustrates the impact of several buffer solution types on fluorescence bursting efficiency while maintaining constant the other reaction conditions, with PBS buffer solution exhibiting the maximum bursting efficiency. Fig. 3E illustrates the fluorescence burst value of the fluorescence sensor system while maintaining constant the reaction conditions and varying the concentration of different monoclonal antibodies. The ideal concentration of monoclonal antibody is 2.0 mg/mL, at which point the fluorescence sensor device achieves its maximum fluorescence burst value and stabilises. Fig. 3F illustrates the fluorescence burst value of the fluorescence sensor system while maintaining constant the reaction conditions and varying antigen concentrations. The ideal antigen concentration is 2.5 mg/mL, as the fluorescence burst value of the fluorescence sensor device attains its maximum and stabilises at this concentration.

3.6. Standard curve for the fluorescence sensor

Samples of fenitrothion at varying concentrations were analysed using an immune-based fluorescence sensor under optimal conditions: pH 7.4, PBS buffer solution, a reaction fluorescence burst duration of 40 min, a competitive fluorescence recovery period of 25 min, an antigen concentration of 2.5 mg/mL and a monoclonal antibody concentration of 2.0 mg/mL. The concentration of fenitrothion was designated as the horizontal axis, while the fluorescence difference F_2-F_1 (where F_1 is the fluorescence value of UCNPs-mAb + GO-Ag and F_2 is the fluorescence value of UCNPs-mAb + GO-Ag + fenitrothion) was assigned to the vertical axis, resulting in a curve showing the correlation between the

fluorescence difference and the fenitrothion concentration. The fluorescence value of the immune-based fluorescence sensor varied with the concentration of fenitrothion, and the standard curves are illustrated in Fig. 4A and Fig. 4B. With the increase in concentration of fenitrothion added to the system, the fluorescence difference F_2-F_1 increased gradually, and the fluorescence difference was positively correlated with the concentration of fenitrothion within the concentration of fenitrothion ranging from 0.1 to 100 ng/mL. The standard curve was $y = 2.80x + 22.23$ ($R^2 = 0.9975$). The limit of detection (LOD) was determined through statistical analysis of the blank signal variation [40]. Following the standard formula $LOD = 3\sigma/k$ (where σ is the standard deviation of 10 replicate blank measurements, and k is the slope of the standard curve), with $\sigma = 0.07587$ and $k = 2.8049$, the calculated LOD was 0.081 ng/mL ($S/N = 3$). Table S1 presents a comparative analysis of various pesticide detection methodologies for fenitrothion. Compared with other methods, the proposed immune-based fluorescence sensor has a lower detection limit and a wider linear range and has the advantages of sensitivity and accuracy in fenitrothion detection.

3.7. Anti-interference experiment

In the anti-interference experiment, K^+ , Ca^{2+} , Sn^{2+} , Mg^{2+} , Cd^{2+} , CrO_4^{2-} , Na^+ , Cu^{2+} , Zn^{2+} , Mn^{2+} , SO_4^{2-} , Cl^- , vitamin C, cysteine, theanine, glutamic acid and glucose were selected from agricultural product samples. 17 different interfering substances at a concentration of 10 $\mu\text{g/mL}$, which is 100 times the concentration of the target analyte fenitrothion. The effects of 17 interfering substances on the sensor's detection of fenitrothion pesticide were analysed to assess the immunofluorescent sensor's anti-interference properties. The results are shown in Fig. S9 and Fig. 4C, the fluorescence difference of the experimental groups before and after the addition of fenitrothion was tested separately, and the results showed that the fluorescence difference of the 17 experimental groups remained relatively consistent with that of the blank group 1. We also calculated the values of tolerance ratio (tolerance ratio = ΔF (addition of interfering substance)/ ΔF (blank group)) for each group, as shown in Table S2, 17 groups with a high concentration (10 $\mu\text{g/mL}$) of interferon had tolerance ratio values ranging from 0.92 to 1.03. The results showed that 17 interfering substances had no effect on

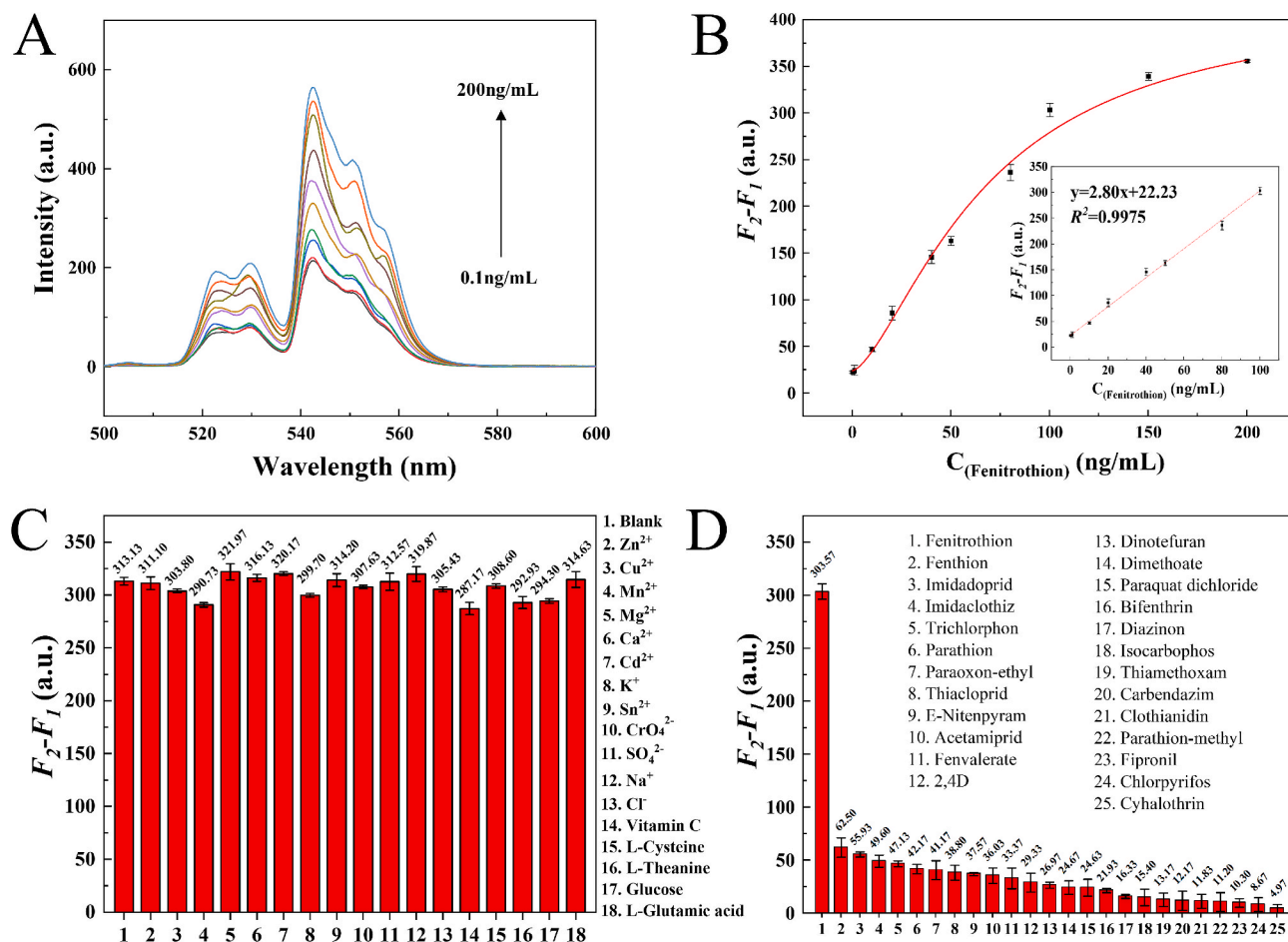


Fig. 4. Trends of fluorescence values of immunofluorescence sensor in relation to fenitrothion concentration (A); The standard curve of fluorescence values of immunofluorescence sensor correlated with fenitrothion concentration (B); The graph of Immuno-type fluorescent sensor anti-interference experimental results (C); Outcomes of specificity experiments conducted with immuno-type fluorescence sensor (D).

the fluorescence difference of the sensor before and after adding fenitrothion, demonstrating the sensor's robust anti-interference performance.

3.8. Specificity experiment

For this study, 25 pesticides were chosen, comprising OPs, organochlorine pesticides, nicotine pesticides, pyrethroids, benzimidazoles and bipyridines. The concentration of all pesticides was 100 ng/mL. Fig. 4D illustrates the outcomes of the specificity experiments. In comparison to the fluorescence recovery value of fenitrothion in curve 1 of the control group, those of the other 25 pesticides were lower. We calculated the tolerance ratio value for the specificity experiment (tolerance ratio = ΔF (pesticide)/ ΔF (fenitrothion)). The results are shown in Table S3, and the tolerance ratio values range from 0.02 to 0.21. These values are much less than 1, indicating that the fluorescence difference ($F_2 - F_1$) of the experimental group is significantly different from that of the fenitrothion group. This proves that the sensor has good specificity. The high specificity is attributed to the monoclonal antibody for fenitrothion employed in this investigation, which exhibits a robust binding affinity for the antigen, while non-fenitrothion insecticides lack the capacity to bind to the antigen, hence preventing any competitive fluorescence recovery effect.

3.9. Spiked recovery experiments

This study aimed to assess the accuracy of the immuno-type

fluorescence sensor by applying to real-life agricultural products treated with fenitrothion pesticide, namely green tea, rice, millet, oleomargarine, cucumber, apple and pear. 7 real samples were tested using the Chinese National Standard gas chromatography-mass spectrometry method (GB23200.93–2016). Fenitrothion pesticide was not detected in any of the samples. Additionally, spiked recovery experiments were conducted on seven groups of real samples, with the results presented in Table 1. Fenitrothion spiked concentrations of 1,40 and 80 ng/mL were used in the experiment. The fenitrothion recoveries in the real samples identified by this immuno-type fluorescence sensor ranged from 91.79 % to 105.43 %, with relative standard deviations (RSDs) between 1.81 % and 10.63 %. The RSDs ranged from 1.81 % to 10.63 %. The fluorescent sensor demonstrated accuracy and sensitivity for the quantification of fenitrothion in real samples, including cereals, vegetables and fruits.

4. Conclusion

This study developed an immuno-type fluorescent sensor utilising the rare earth upconversion nanomaterials $\text{NaYF}_4:\text{Yb},\text{Er}@/\text{NaYF}_4$ and GO, employing FRET and competitive reactions for the quantitative detection of fenitrothion pesticide in agricultural products. The method exhibits great accuracy with a linear range of 0.1 to 100 ng/mL and a detection limit of 0.081 ng/mL. The sensor exhibits high specificity due to the competitive interaction between the monoclonal antibody and the specific binding of the antigen to the target detector, resulting in low fluorescence response from the 25 nontarget pesticides examined in this study. The sensor exhibits exceptional resistance to 17 prevalent

Table 1
Results of spiked recovery experiments.

Sample	Spiked value (ng/mL)	Measured value (ng/mL)	Average recovery (%)	Relative standard deviation (%)
Green tea	1	0.98 ± 0.06	97.74	6.21
	40	37.78 ± 0.90	94.44	2.38
	80	77.69 ± 0.28	97.11	2.94
Rice	1	1.01 ± 0.04	101.31	4.40
	40	38.36 ± 1.15	95.90	3.00
	80	84.35 ± 1.95	105.43	2.31
Millet	1	1.03 ± 0.08	102.50	7.53
	40	40.70 ± 4.05	101.76	9.95
	80	81.30 ± 3.94	101.62	4.85
Romaine lettuce	1	0.93 ± 0.02	92.98	1.81
	40	40.75 ± 0.95	101.88	2.33
	80	82.30 ± 5.04	102.87	6.12
Cucumber	1	1.04 ± 0.07	103.69	7.08
	40	41.20 ± 2.16	103.01	5.24
	80	81.31 ± 1.87	101.64	2.29
Apple	1	0.99 ± 0.11	98.93	10.63
	40	40.48 ± 0.87	101.19	2.16
	80	81.50 ± 4.06	101.88	4.98
Pear	1	0.92 ± 0.05	91.79	5.50
	40	40.51 ± 3.62	101.28	8.93
	80	79.66 ± 2.27	99.57	2.86

interferences in agricultural goods, including ions, amino acids and vitamins. The sensor is employed for the spiking recovery assessment of fenitrothion in seven types of real agricultural products, yielding spiked recoveries between 91.79 % and 105.43 %, with RSDs ranging from 1.81 % to 10.63 %. Therefore, the immuno-type fluorescent sensor is a rapid detection technique for identifying fenitrothion in agricultural products, characterised by high efficiency, sensitivity, specificity and accuracy. In addition, this study offers innovative concepts, methodologies and technical approaches for developing biosensors aimed at detecting other pesticide residues and environmental pollutants utilising UCNPs.

CRediT authorship contribution statement

Konghao Peng: Writing – review & editing, Methodology, Investigation, Data curation. **Anqi Bai:** Writing – review & editing, Methodology, Investigation, Data curation. **Yue Wu:** Formal analysis. **Shihan Wang:** Conceptualization. **Heran Gao:** Formal analysis. **Shurong Li:** Resources. **Lingyan Zhang:** Formal analysis. **Min Jin:** Validation. **Wei Peng:** Writing – review & editing. **Peijun Meng:** Writing – review & editing, Supervision, Project administration, Funding acquisition.

Declaration of competing interest

The authors declare that they have no known competing financial interests or personal relationships that could have appeared to influence the work reported in this paper.

Acknowledgments

This work was supported by the National Natural Science Foundation of China (No. 82360656 and 81960601), the Program for Young Talents of Science and Technology in Universities of Inner Mongolia Autonomous Region (NJYT23026), and the Natural Science Foundation of Inner Mongolia Autonomous Region of China (2023MS08009).

Appendix A. Supplementary data

Supplementary data to this article can be found online at <https://doi.org/10.1016/j.microc.2025.113573>.

Data availability

Data will be made available on request.

References

- [1] L. Wei, N. Zhu, X. Liu, H. Zheng, K. Xiao, Q. Huang, H. Liu, M. Cai, Application of Hi-throat/Hi-volume SPE technique in assessing organophosphorus pesticides and their degradation products in surface water from Tai Lake, east China, *J. Environ. Manage.* 1 (305) (2022 Mar) 114346, <https://doi.org/10.1016/j.jenvman.2021.114346>.
- [2] P. Kumar, M. Arshad, A. Gacem, S. Soni, S. Singh, M. Kumar, V.K. Yadav, M. Tariq, R. Kumar, D. Shah, S.G. Wanale, M.K.M. Al Mesfer, J.K. Bhutto, K.K. Yadav, Insight into the environmental fate, hazard, detection, and sustainable degradation technologies of chlorpyrifos-an organophosphorus pesticide, *Environ. Sci. Pollut. Res. Int.* 30 (50) (2023 Oct) 108347–108369, <https://doi.org/10.1007/s11356-023-30049-y>.
- [3] C. Ssemugabo, A. Bradman, J.C. Ssempebwa, F. Sillé, D. Guwatudde, An assessment of health risks posed by consumption of pesticide residues in fruits and vegetables among residents in the Kampala Metropolitan Area in Uganda, *Int. J. Food Contam.* 9 (1) (2022) 4, <https://doi.org/10.1186/s40550-022-00090-9>.
- [4] L.B. Merga, A.A. Mengistie, M.T. Alemu, P.J. Van den Brink, Biological and chemical monitoring of the ecological risks of pesticides in Lake Ziway, Ethiopia, *Chemosphere.* 266 (2021 Mar) 129214, <https://doi.org/10.1016/j.chemosphere.2020.129214>.
- [5] J. Chen, S. Zhao, S. Wesseling, N.I. Kramer, I.M.C.M. Rietjens, H. Bouwmeester, Acetylcholinesterase Inhibition in Rats and Humans Following Acute Fenitrothion Exposure Predicted by Physiologically Based Kinetic Modeling-Facilitated Quantitative *In Vitro* to *In Vivo* Extrapolation, *Environ. Sci. Tech.* 57 (49) (2023 Dec 12) 20521–20531, <https://doi.org/10.1021/acs.est.3c07077>.
- [6] G. Yu, Y. Li, T. Jian, L. Shi, S. Cui, L. Zhao, X. Jian, B. Kan, Clinical Analysis of Acute Organophosphorus Pesticide Poisoning and Successful Cardiopulmonary Resuscitation: A Case Series, *Front. Public Health* 27 (10) (2022 May) 866376, <https://doi.org/10.3389/fpubh.2022.866376>.
- [7] V.E. Sobolev, M.O. Sokolova, R.O. Jenkins, N.V. Goncharov, Molecular Mechanisms of Acute Organophosphate Nephrotoxicity, *Int. J. Mol. Sci.* 23 (16) (2022 Aug 9) 8855, <https://doi.org/10.3390/ijms23168855>.
- [8] K. Seebunrueng, S. Tamuang, P. Jarujamrus, S. Saengsuwan, N. Patdhanagul, Y. Areeerob, S. Sansuk, S. Srijaranai, Eco-friendly thermosensitive magnetic-molecularly-imprinted polymer adsorbent in dispersive solid-phase microextraction for gas chromatographic determination of organophosphorus pesticides in fruit samples, *Food Chem.* 1 (430) (2024 Jan) 137069, <https://doi.org/10.1016/j.foodchem.2023.137069>.
- [9] E. Yildiz, H. Çabuk, Dispersive liquid-liquid microextraction method combined with sugaring-out homogeneous liquid-liquid extraction for the determination of some pesticides in molasses samples, *J. Sep. Sci.* 44 (22) (2021 Nov) 4151–4166, <https://doi.org/10.1002/jssc.202100551>.
- [10] N. Sharma, P. Thakur, M.G. Chaskar, Determination of eight endocrine disruptor pesticides in bovine milk at trace levels by dispersive liquid-liquid microextraction followed by GC-MS determination, *J. Sep. Sci.* 44 (15) (2021 Aug) 2982–2995, <https://doi.org/10.1002/jssc.202100183>.
- [11] Z. Shu, Y. Zou, X. Wu, et al., NH₂-MIL-125(Ti)/Reduced Graphene Oxide Enhanced Electrochemical Detection of Fenitrothion in Agricultural Products, *Foods.* 12 (7) (2023) 1534, <https://doi.org/10.3390/foods12071534>.
- [12] T. Lv, B. Wang, N. Xu, B. Shang, N. Liu, C. Su, C. Yang, H. Li, Z. Xu, C. Sun, Gold nanoclusters-manganese dioxide composite-based fluorescence immunoassay for sensitive monitoring of fenitrothion degradation in Chinese cabbage, *Food Chem.* 30 (412) (2023 Jun) 135551, <https://doi.org/10.1016/j.foodchem.2023.135551>.

- [13] S.M. Badawy, Validation and kinetic of enzymatic method for the detection of organophosphate insecticides based on cholinesterase inhibition, *Toxicol. Mech. Methods* 30 (2) (2020 Feb) 134–138, <https://doi.org/10.1080/15376516.2019.1669248>.
- [14] C.L. Yang, L.H. Yu, Y.H. Pang, X.F. Shen, A ratiometric fluorescence sensor for detection of organophosphorus pesticides based on enzyme-regulated multifunctional Fe-based metal-organic framework, *Talanta* 1 (278) (2024 Oct) 126516, <https://doi.org/10.1016/j.talanta.2024.126516>.
- [15] F. Liu, T. Lei, Y. Zhang, Y. Wang, Y. He, A BCNO QDs-MnO₂ nanosheets based fluorescence “off-on-off” and colorimetric sensor with smartphone detector for the detection of organophosphorus pesticides, *Anal. Chim. Acta* 1 (1184) (2021 Nov) 339026, <https://doi.org/10.1016/j.aca.2021.339026>.
- [16] F. Zhang, Y. Ma, Y. Chi, H. Yu, Y. Li, T. Jiang, X. Wei, J. Shi, Self-assembly, optical and electrical properties of perylene diimide dyes bearing unsymmetrical substituents at bay position, *Sci. Rep.* 8 (1) (2018 May 29) 8208, <https://doi.org/10.1038/s41598-018-26502-5>.
- [17] Y. Liang, T. Zhang, M. Tang, Toxicity of quantum dots on target organs and immune system, *J. Appl. Toxicol.* 42 (1) (2022 Jan) 17–40, <https://doi.org/10.1002/jat.4180>.
- [18] C. Bai, M. Tang, Progress on the toxicity of quantum dots to model organism-zebrafish, *J. Appl. Toxicol.* 43 (1) (2023 Jan) 89–106, <https://doi.org/10.1002/jat.4333>.
- [19] Y. Li, C. Chen, F. Liu, J. Liu, Engineered lanthanide-doped upconversion nanoparticles for biosensing and bioimaging application, *Mikrochim. Acta* 189 (3) (2022 Feb 17) 109, <https://doi.org/10.1007/s00604-022-05180-1>.
- [20] K. Malhotra, D. Hrovat, B. Kumar, G. Qu, J.V. Houten, R. Ahmed, P.A.E. Pinnoo, P. T. Gunning, U.J. Krull, Lanthanide-Doped Upconversion Nanoparticles: Exploring A Treasure Trove of NIR-Mediated Emerging Applications, *ACS Appl. Mater. Interfaces* 15 (2) (2023 Jan 18) 2499–2528, <https://doi.org/10.1021/acsami.2c12370>.
- [21] M. He, N. Shang, Q. Zhu, J. Xu, Paper-based upconversion fluorescence aptasensor for the quantitative detection of immunoglobulin E in human serum, *Anal. Chim. Acta* 1143 (2021) 93–100, <https://doi.org/10.1016/j.aca.2020.11.036>.
- [22] Y. Rong, H. Li, Q. Ouyang, S. Ali, Q. Chen, Rapid and sensitive detection of diazinon in food based on the FRET between rare-earth doped upconversion nanoparticles and graphene oxide, *Spectrochim. Acta A Mol. Biomol. Spectrosc.* 5 (239) (2020 Oct) 118500, <https://doi.org/10.1016/j.saa.2020.118500>.
- [23] G. Gopal, N. Roy, A. Mukherjee, Recent Developments in the Applications of GO/rGO-Based Biosensing Platforms for Pesticide Detection, *Biosensors (basel)*. 13 (4) (2023 Apr 19) 488, <https://doi.org/10.3390/bios13040488>.
- [24] M. Arvand, A.A. Mirroshandel, Highly-sensitive aptasensor based on fluorescence resonance energy transfer between l-cysteine capped ZnS quantum dots and graphene oxide sheets for the determination of edifenphos fungicide, *Biosens. Bioelectron.* 15 (96) (2017 Oct) 324–331, <https://doi.org/10.1016/j.bios.2017.05.028>.
- [25] Y. Wang, M. Lv, Z. Chen, Z. Deng, N. Liu, J. Fan, W. Zhang, A Fluorescence Resonance Energy Transfer Probe Based on DNA-Modified Upconversion and Gold Nanoparticles for Detection of Lead Ions, *Front. Chem.* 21 (8) (2020 Apr) 238, <https://doi.org/10.3389/fchem.2020.00238>.
- [26] Y. Liu, Y. Xiao, Y. Zhang, X. Gao, H. Wang, B. Niu, W. Li, ZnO-rGO-based electrochemical biosensor for the detection of organophosphorus pesticides, *Bioelectrochemistry* 156 (2024 Apr) 108599, <https://doi.org/10.1016/j.bioelechem.2023.108599>.
- [27] W. Ahmad, L. Wang, M. Zareef, Q. Chen, Ultrasensitive detection of *Staphylococcus aureus* using a non-fluorescent cDNA-grafted dark BBQ®-650 chromophore integrated hydrophilic upconversion nanoparticles/aptamer system, *Mikrochim. Acta*. 190 (7) (2023 Jun 6) 250, <https://doi.org/10.1007/s00604-023-05823-x>.
- [28] M. Liu, J. Wei, Y. Wang, H. Ouyang, Z. Fu, Dopamine-functionalized upconversion nanoparticles as fluorescent sensors for organophosphorus pesticide analysis, *Talanta* 1 (195) (2019 Apr) 706–712, <https://doi.org/10.1016/j.talanta.2018.11.105>.
- [29] S. Farooq, H. Aziz, S. Ali, G. Murtaza, M. Rizwan, M.H. Saleem, S. Mahboob, K. A. Al-Ghanim, M.N. Riaz, B. Murtaza, Synthesis of Functionalized Carboxylated Graphene Oxide for the Remediation of Pb and Cr Contaminated Water, *Int. J. Environ. Res. Public Health* 19 (17) (2022 Aug 25) 10610, <https://doi.org/10.3390/ijerph191710610>.
- [30] F. Si, R. Zou, S. Jiao, X. Qiao, Y. Guo, G. Zhu, Inner filter effect-based homogeneous immunoassay for rapid detection of imidacloprid residue in environmental and food samples, *Ecotoxicol. Environ. Saf.* 148 (2018) 862–868, <https://doi.org/10.1016/j.ecoenv.2017.11.062>.
- [31] Y. Guo, R. Zou, F. Si, W. Liang, T. Zhang, Y. Chang, X. Qiao, J. Zhao, A sensitive immunoassay based on fluorescence resonance energy transfer from up-converting nanoparticles and graphene oxide for one-step detection of imidacloprid, *Food Chem.* 15 (335) (2021 Jan) 127609, <https://doi.org/10.1016/j.foodchem.2020.127609>.
- [32] Yahui Li, Yanxiao Li, Di Zhang, Weilong Tan, Jiyong Shi, Zhihua Li, Hanyu Liu, Yinyin Yu, Liu Yang, Xin Wang, Yunyun Gong, Xiaobo Zou. A fluorescence resonance energy transfer probe based on functionalized graphene oxide and upconversion nanoparticles for sensitive and rapid detection of zearalenone. *Lwt*, 2021, 147, 111541. <https://doi.org/10.1016/j.lwt.2021.111541>.
- [33] Y. Zhang, B. Duan, Q. Bao, T. Yang, T. Wei, J. Wang, C. Mao, C. Zhang, M. Yang, Aptamer-modified sensitive nanobiosensors for the specific detection of antibiotics, *J. Mater. Chem. B* 8 (37) (2020 Sep 30) 8607–8613, <https://doi.org/10.1039/d0tb01441a>.
- [34] R. Zou, Y. Chang, T. Zhang, F. Si, Y. Liu, Y. Zhao, Y. Liu, M. Zhang, X. Yu, X. Qiao, G. Zhu, Y. Guo, Up-Converting Nanoparticle-Based Immunochromatographic Strip for Multi-Residue Detection of Three Organophosphorus Pesticides in Food, *Front. Chem.* 7 (7) (2019 Feb) 18, <https://doi.org/10.3389/fchem.2019.00018>.
- [35] H. Song, H. Zhou, Q. Zhuang, Z. Li, F. Sun, Z. Yuan, Y. Lou, G. Zhou, Y. Zhao, IFE based nanosensor composed of UCNPs and Fe(II)-phenanthroline for detection of hypochlorous acid and periodic acid, *J. Rare Earths* 41 (2) (2023) 200–207, <https://doi.org/10.1016/j.jre.2022.04.005>.
- [36] W. Yang, M. Cao, Study on the difference in adsorption performance of graphene oxide and carboxylated graphene oxide for Cu(II), Pb(II) respectively and mechanism analysis, *Diam. Relat. Mater.* 129 (2022) 109332, <https://doi.org/10.1016/j.diamond.2022.109332>.
- [37] J. Ghitman, E.I. Biru, E. Cojocar, G.G. Pircalabioru, E. Vasile, H. Iovu, Design of new bioinspired GO-COOH decorated alginate/gelatin hybrid scaffolds with nanofibrous architecture: structural, mechanical and biological investigations, *RSC Adv.* 11 (22) (2021 Apr 13) 13653–13665, <https://doi.org/10.1039/d1ra01432c>.
- [38] M. Srikaew, Y. Wongnongwa, S. Jungsuitiwong, C. Kaiyasuan, V. Promarak, S. Saengsuwan, Improvement of adsorption performance and selectivity of GO-COOH towards MB dye through effective carboxylation approach: Combined experimental and DFT studies, *Colloids Surf A Physicochem Eng Asp* 673 (2023) 131920, <https://doi.org/10.1016/j.colsurfa.2023.131920>.
- [39] Y. Shen, Y. Chen, H. Wang, X. Zhao, Lu. Haixia, J. Zhu, Immunochromatographic assay integrated smartphone-based device for simultaneous detection of multiple mycotoxins using core-shell up-conversion nanoparticles, *Sens. Actuators B* 398 (2024) 134783, <https://doi.org/10.1016/j.snb.2023.134783>.
- [40] Q. Chen, R. Sheng, P. Wang, Q. Ouyang, A. Wang, S. Ali, M. Zareef, M.M. Hassan, Ultra-sensitive detection of malathion residues using FRET-based upconversion fluorescence sensor in food, *Spectrochim. Acta A Mol. Biomol. Spectrosc.* 5 (241) (2020 Nov) 118654, <https://doi.org/10.1016/j.saa.2020.118654>.